Erzincan Üniversitesi
Fen Bilimleri Enstitüsü Dergisi
2025, 18(2), 431-450
ISSN: 1307-9085, e-ISSN: 2149-4584
Araştırma Makalesi

Erzincan University
Journal of Science and Technology
2025, 18(2), 431-450
DOI: 10.18185/erzifbed.1673054
Research Article

First-Ever Use of $LiMn_2O_4$ Cathode in State-of-the-Art Ammonium-Ion Batteries: Unlocking a New Ametal Charge Carrier

Melisa Uçan[1], Dilara Özgenç[1], Yıldıray Topcu[1], Burak Tekin[1]*

[1,] *Ondokuz Mayis University, Faculty of Engineering, Chemical Engineering Department, Atakum, Samsun, 55139, Turkey.

Received: 12/04/2025, **Revised:** 16/06/2025, **Accepted:** 24/06/2025, **Published:** 31/08/2025

Abstract

Growing demand for sustainable, economical, and high-efficiency energy storage has intensified research into aqueous ammonium-ion battery systems. These electrochemical storage devices offer inherent safety benefits, environmental compatibility, and cost advantages stemming from ammonium ions' favorable characteristics - their lightweight nature (18 $gmol^{-1}$) and minimal solvated dimensions (~1.25 Å). A critical research gap exists in developing cathode materials that can stably cycle NH_4^+ ions in water-based electrolytes. Our investigation focuses on spinel-phase lithium manganese oxide ($LiMn_2O_4$) as a potential NH_4^+ host material, leveraging its distinctive structural advantages. The material's face-centered cubic framework with three-dimensional lithium diffusion pathways enables rapid ionic conduction and stable electrochemical behavior. Beyond its performance merits, $LiMn_2O_4$ stands out for its economical precursor materials and reduced environmental impact compared to standard cathode compounds. The material's theoretical energy storage capability reaches approximately 148 mAh g^{-1}, indicating significant potential for energy-dense battery designs. We employed solid-state synthesis at elevated temperatures to produce the material, with XRD analysis verifying the development of an orthorhombic crystalline phase. Electrochemical analysis using cyclic voltammetry indicated a two-step lithium extraction process in ammonium-ion electrolytes. As cycling progressed, redox peaks associated with ammonium-ion insertion and extraction became more defined, highlighting the material's capability for efficient and reversible charge storage. Galvanostatic charge-discharge tests revealed that the $LiMnO_2$-based electrode delivered a stable specific capacity of approximately 47 mAh g^{-1} during NH_4^+ intercalation/de-intercalation. The study demonstrates that $LiMn_2O_4$ effectively supports ammonium-ion storage, offering a sustainable and high-performance cathode option for next-generation aqueous batteries. These findings provide crucial insights into the material's electrochemical behavior and potential for advancing ammonium-ion battery technology.

Keywords: The state-of-art aqueous ammonium-ion batteries, Spinel $LiMn_2O_4$ host structure, Electrochemical energy storage

$LiMn_2O_4$ Katodunun Çığır Açan İlk Kullanımı: Yeni Nesil Amonyum-İyon Pillerde Metal Olmayan Bir Taşıyıcının Kilidini Açmak

Öz

Düşük maliyetli, yüksek performanslı ve çevre dostu enerji depolama çözümlerine yönelik arayış, sulu amonyum-iyon pillerine olan ilgiyi artırmıştır. Bu sistemler, amonyum iyonlarının düşük molar kütlesi ve küçük hidrate iyon yarıçapı sayesinde gelişmiş güvenlik, sürdürülebilirlik ve uygun maliyet sunar. Ancak, sulu elektrolitlerde geri dönüşümlü amonyum-iyon depolayabilen bir katot malzemesinin belirlenmesi önemli bir zorluk olarak kalmaktadır. Bu çalışma, lityum manganez oksidi ($LiMn_2O_4$) amonyum-iyon pilleri için umut verici bir katot malzemesi olarak incelemektedir. Kübik simetriye ve birbirine bağlı 3D iyon difüzyon kanallarına sahip spinel $LiMn_2O_4$ yapısı, verimli yük taşınımı ve sağlam elektrokimyasal performans sağlar. Ayrıca, düşük maliyetli hammaddeler ve çevresel avantajlar, bu malzemeyi geleneksel geçiş metal oksitlerine

*Corresponding Author: burak.tekin@omu.edu.tr
Melisa UÇAN, https://orcid.org/0009-0004-9188-889X
Dilara ÖZGENÇ, https://orcid.org/0009-0000-4473-4178
Yıldıray TOPCU, https://orcid.org/0000-0002-2095-6603
Burak TEKİN, https://orcid.org/0000-0002-7533-3008

cazip bir alternatif haline getirir. ~148 mAh g^{-1} teorik kapasitesiyle $LiMn_2O_4$, önemli özgül kapasite sergileyerek pil enerji yoğunluğunun artmasına katkıda bulunur. Malzeme, yüksek sıcaklıkta katı hal reaksiyonu ile sentezlenmiş ve X-ışını kırınımı (XRD) ile kararlı bir ortorombik yapının oluştuğu doğrulanmıştır. Döngüsel voltametri kullanılarak yapılan elektrokimyasal analiz, amonyum-iyon elektrolitlerinde iki aşamalı bir lityum çıkarma sürecini ortaya koymuştur. İlerleyen döngülerde, amonyum-iyon yerleşimi ve çıkarımıyla ilişkili redoks tepkimelerinin daha belirgin hale gelmesi, malzemenin verimli ve geri dönüşümlü yük depolama yeteneğini vurgulamaktadır. Galvanostatik şarj-deşarj testleri, Mn_2O_4 bazlı elektrodun NH_4^+ yerleşimi/çıkarımı sırasında yaklaşık 47 $mAhg^{-1}$ kararlı özgül kapasite sağladığını göstermiştir. Bu çalışma, $LiMn_2O_4$'ün amonyum-iyon depolamayı etkin bir şekilde desteklediğini ve yeni nesil sulu piller için sürdürülebilir ve yüksek performanslı bir katot seçeneği sunduğunu kanıtlamaktadır. Bu bulgular, malzemenin elektrokimyasal davranışı ve amonyum-iyon pil teknolojisinin ilerlemesindeki potansiyeli hakkında kritik bilgiler sağlar.

Anahtar Kelimeler: Yeni nesil sulu amonyum iyon bataryalar, Spinel $LiMn_2O_4$ barinak yapi, Elektrokimyasal Enerji depolama

1. Introduction

The global energy demand has long been met predominantly by fossil fuels. However, their finite nature and rapid depletion due to excessive human consumption pose a serious challenge for future energy security. Additionally, fossil fuel combustion is a primary driver of climate change, releasing greenhouse gases that accelerate global warming [1]. Consequently, there is an urgent need for clean, sustainable, and renewable energy sources. Among the alternatives, solar, wind, and tidal energy stand out due to their abundance and eco-friendliness [2]. However, their inherent intermittency, driven by environmental conditions, leads to fluctuating energy output [3]. Since modern society relies on a stable and uninterrupted energy supply, integrating efficient energy storage systems with renewable sources becomes imperative. At this point, fuel cells, batteries, and capacitors emerge as potential candidates for energy storage. An ideal energy storage system should exhibit high energy density, high power density, and fast charge/discharge capabilities [4-6]. As depicted in the Ragone plot, batteries strike an optimal balance between these key performance metrics, offering a superior combination of energy density and power output, along with relatively short charging times (Figure 1a) [7-9]. This makes them a highly attractive solution for ensuring a stable and reliable energy supply in a future powered by renewable sources. The rapid worldwide adoption of clean energy technologies has created unprecedented demand for high-performance energy storage solutions. Among the available technologies, batteries stand out as a highly viable option due to their ability to store and deliver energy with high efficiency [10]. However, the development of battery technology has been a continuous process of innovation, driven by the increasing demand for higher energy density, faster charging, and improved sustainability.

Figure 1b illustrates the historical evolution of rechargeable batteries, highlighting key advancements over time. The timeline begins with lead-acid batteries, introduced in the 1860s, which provided a foundational energy storage solution despite their limited energy density (~30 $Whkg^{-1}$). In the early 1900s, nickel-cadmium (Ni-Cd) batteries emerged, offering improved

energy density (60 $Whkg^{-1}$) and enhanced cycle life, making them suitable for portable applications. The 1960s saw the development of nickel-metal hydride (Ni-MH) batteries, which further increased energy density (80 $Whkg^{-1}$) and reduced environmental concerns. However, the most transformative breakthrough came in the 1990s with the commercialization of lithium-ion (Li-ion) batteries, which revolutionized energy storage by delivering a significantly higher energy density (~180 $Whkg^{-1}$) and greater efficiency [11-15]. During the last decade, cutting-edge battery systems utilizing lithium chemistry saw significant technological progress, facilitating their broad implementation across portable devices, EV platforms, and utility-scale storage applications. Despite these advancements, conventional battery technologies, particularly lithium-ion batteries, still face critical challenges such as flammability, toxicity, and material scarcity [16, 17]. To address these concerns, researchers are exploring alternative battery chemistries that prioritize safety, environmental friendliness, and cost-effectiveness. Among these, aqueous ammonium-ion batteries have emerged as a promising solution due to their non-flammable water-based electrolytes, low toxicity, and reduced risk of electrode corrosion. These next-generation batteries offer a safer and more sustainable approach to energy storage, making them an attractive candidate for future large-scale applications in renewable energy integration and beyond [18-20].

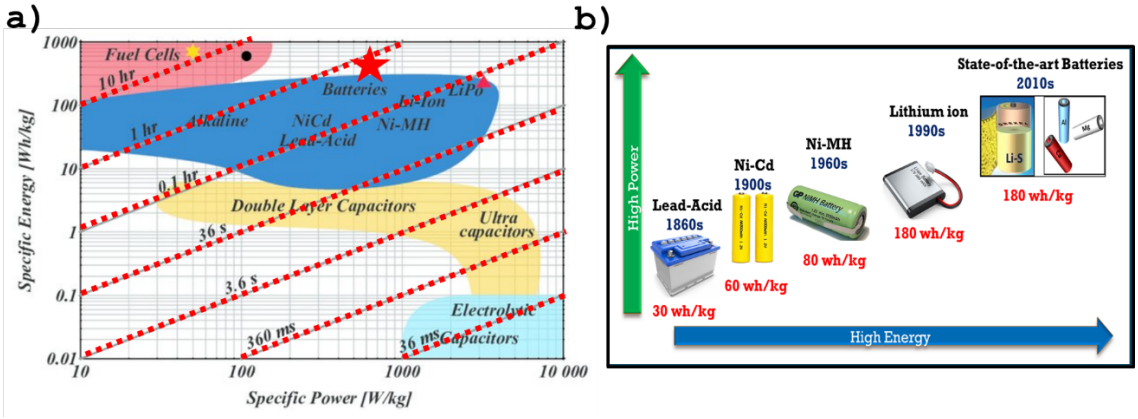

Figure 1. a) Ragon plot diagram that compares different energy storage technologies in terms of specific power, specific energy and charging time, b) Time-line of rechargeable batteries.

Aqueous batteries have emerged as a promising alternative to conventional non-aqueous batteries, primarily to mitigate safety concerns associated with flammable and explosive organic electrolytes (Figure 2) [21-24]. Unlike non-aqueous systems, aqueous batteries utilize water-based electrolytes, which eliminate the risks of fire hazards while also offering advantages such as faster ion transport, the absence of a solid electrolyte interphase (SEI) layer, and cost-effective electrolyte materials. However, despite their safety benefits, aqueous batteries are inherently challenged by issues such as passivation, corrosion, and dendrite formation [25-28]. These problems arise due to the metallic characteristics of electrodes and charge carriers, leading to undesirable side reactions that hinder battery performance and longevity. To overcome these limitations, the recently developed aqueous ammonium-ion battery presents a novel approach by utilizing metal-free charge carriers. This innovation not only resolves the flammability and toxicity issues of non-aqueous batteries but also significantly

mitigates the intrinsic challenges of aqueous systems [29]. The absence of metal-based charge carriers prevents dendrite growth, minimizes corrosion-related degradation, and eliminates passivation layers that could hinder ion mobility [30]. As a result, aqueous ammonium-ion batteries represent a major step forward in achieving safe, high-performance, and long-lasting energy storage solutions, making them a strong candidate for future applications in grid storage, electric mobility, and renewable energy integration.

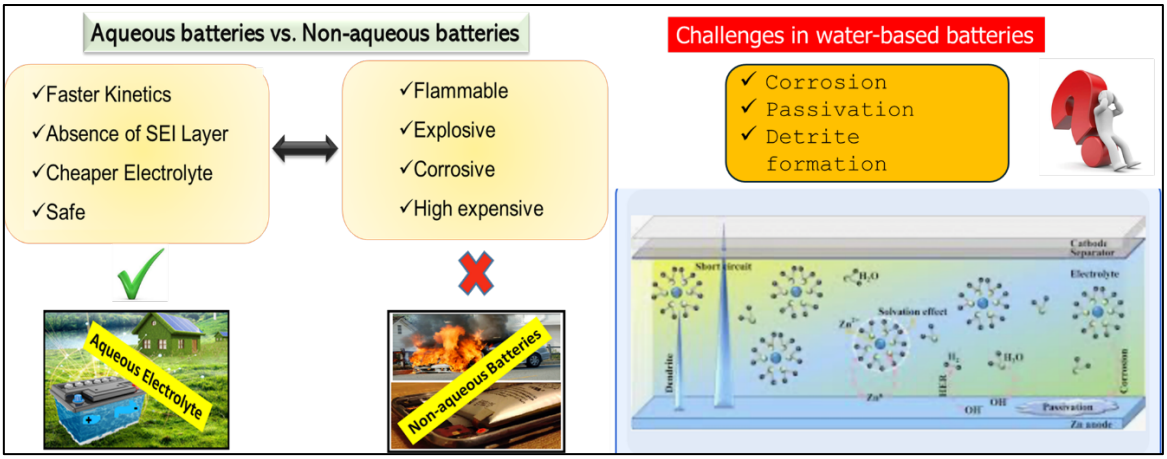

Figure 2. Merits of aqueous rechargeable batteries over non-aqueous batteries, and challenges of water-based batteries.

The ammonium cation (NH_4^+) possesses unique electrochemical properties that render it particularly suitable for energy storage systems. Its lightweight nature (molecular weight: 18 $gmol^{-1}$) combined with compact solvation geometry (hydrated radius ≈1.25 Å) promotes fast ionic mobility within electrode structures, while simultaneously supporting elevated capacity potential in battery configurations. Moreover, its proton-coupled redox behavior enhances charge transfer mechanisms, potentially improving electrochemical performance. In addition to these intrinsic properties, ammonium salts are cost-effective, non-toxic, and naturally abundant, further supporting the feasibility of ammonium-ion batteries (AIBs) for large-scale energy storage [29, 31, 32]. Despite these advantages, the development of AIBs remains in its nascent stages, primarily due to the absence of electrode materials that can reversibly and stably accommodate NH_4^+ intercalation. Current research efforts have focused on various cathode materials, including Prussian blue analogs [33-35], organic polymers [36, 37], and transition metal oxides [38, 39]. However, many of these materials exhibit limitations such as inadequate capacity retention, poor cycling stability, or sluggish ion diffusion kinetics. Addressing these challenges through the design of advanced electrode architectures and the optimization of electrolyte compositions is essential for realizing the full potential of AIBs in next-generation energy storage systems.

Among potential cathode materials, spinel lithium manganese oxide ($LiMn_2O_4$) stands out due to its well-documented performance in LIBs and its structural adaptability to different charge carriers [40, 41]. $LiMn_2O_4$ possesses a three-dimensional (3D) spinel framework with interconnected diffusion channels that facilitate rapid ion transport, while the Mn^{3+}/Mn^{4+} redox couple provides a high theoretical capacity of ~148 mAh g^{-1} [41]. The material is also cost-

effective and environmentally benign, as manganese is more abundant and less toxic than cobalt or nickel [43]. Recent studies have demonstrated that $LiMn_2O_4$ can accommodate other monovalent ions, such as Na^+ and K^+, suggesting its potential compatibility with NH_4^+ [44, 45]. However, the use of $LiMn_2O_4$ in AIBs has not been previously explored, leaving a critical gap in understanding its electrochemical behavior in NH_4^+-based electrolytes.

This work examines $LiMn_2O_4$'s previously unreported application as an electrode material in ammonium-ion aqueous batteries. The spinel-phase material was synthesized through calcination of stoichiometric precursors, with crystallographic verification by XRD analysis. Systematic electrochemical testing, comprising both potential-sweep and constant-current methods, established stable NH_4^+ (de)intercalation behavior with maintained capacity retention during cycling. Our findings demonstrate that $LiMn_2O_4$ is a viable cathode material for AIBs, offering a sustainable and high-performance alternative to existing systems. This work not only expands the range of available materials for NH_4^+ storage but also provides foundational insights into the electrochemical mechanisms governing NH_4^+ intercalation in spinel oxides. Future research should focus on optimizing electrolyte formulations, exploring doping strategies to enhance conductivity, and integrating $LiMn_2O_4$ into full-cell configurations with compatible anode materials. By addressing these challenges, AIBs could emerge as a competitive technology for grid-scale storage and other applications where safety, cost, and sustainability are paramount.

2. Material and Methods

2.1. Synthesis procedure

Orthorhombic $LiMn_2O_4$ was prepared using a sol-gel approach with lithium hydroxide monohydrate ($LiOH \cdot H_2O$) and manganese acetate tetrahydrate ($Mn(CH_3COO)_2 \cdot 4H_2O$) as starting materials (Figure 3). Initially, stoichiometric amounts of $LiOH \cdot H_2O$ and $Mn(CH_3COO)_2 \cdot 4H_2O$ were dissolved separately in deionized water under magnetic stirring. Citric acid was introduced as a complexing agent, and the mixture was maintained at 50 °C with constant agitation. The pH was carefully adjusted to 8.0 using NH_4OH, monitored via a calibrated pH meter. The solution was then heated to 80 °C under stirring to promote gel formation. The resulting viscous gel was dried at 110 °C for 24 h to eliminate residual moisture. To remove organic impurities and initiate crystallization, the dried precursor was calcined at 450 °C for 4 h. Finally, high-temperature sintering at 780 °C for 12 h yielded the crystalline $LiMn_2O_4$ phase. The product was subsequently analyzed for structural and electrochemical performance.

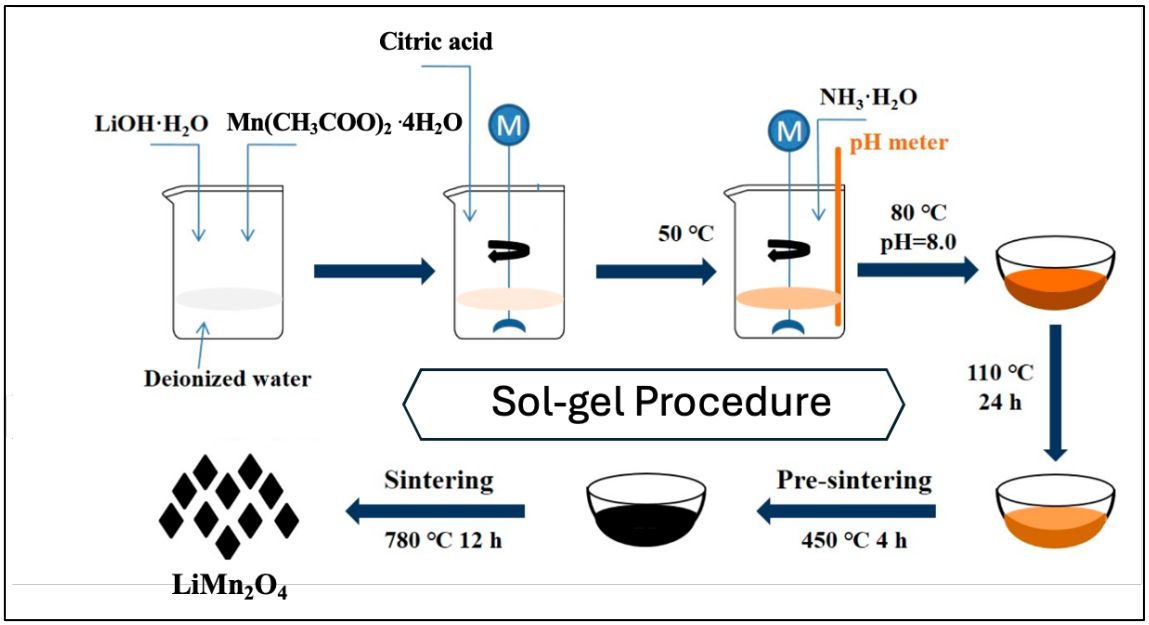

Figure 3. Schematic illustration of $LiMn_2O_4$ synthesis procedure using the sol-gel method.

2.2. Electrode Preparation

The cathode slurry was prepared by combining active material ($LiMn_2O_4$), conductive carbon (Super P), and PVDF binder in an 80:10:10 weight ratio. These components were homogenized in NMP solvent using a planetary mixer for 2 h to achieve a uniform dispersion. The resulting slurry was doctor-bladed onto graphite current collectors using a 150 µm gap applicator. The coated electrodes were vacuum-dried at 70 °C for 12 h to ensure complete solvent removal and optimal adhesion (Figure 4).

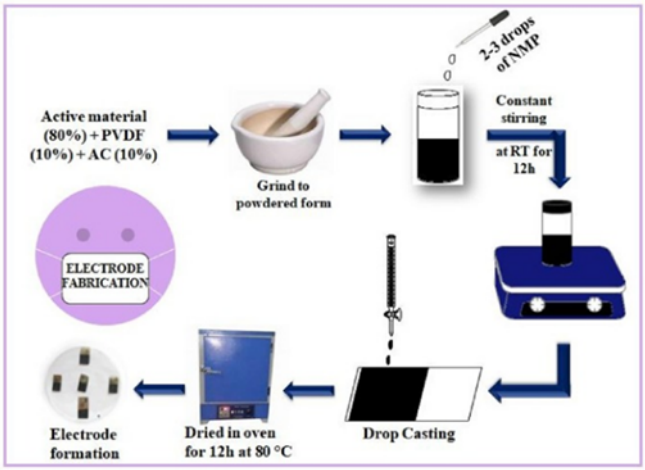

Figure 4. Workflow for preparing the electrode slurry and coating onto graphite substrate.

2.3. Electrochemical Cell Assembly and Measurements

The experimental setup employed a standard three-electrode configuration with the following components:

- Active electrode: Spinel $LiMn_2O_4$ (surface area = 0.75 cm^2)
- Auxiliary electrode: Graphite rod (99.99% purity)
- Potential reference: Standard Ag/AgCl electrode

The electrochemical cell contained an optimized 0.5 molar ammonium sulfate solution as the ionic conductor, chosen for its exceptional potential window stability. Potential-dependent current responses were measured through cyclic polarization experiments spanning 0.0–1.2 V versus the reference electrode, with voltage scan rates incrementally increased from 1 to 10 millivolts per second. Charge storage performance was assessed through rate capability tests at current loads ranging from 148 to 1480 milliamperes per gram (corresponding to 1C–10C rates), with continuous cycling over 100 iterations. Electrochemical Impedance analysis was performed via small-signal impedance measurements, covering five orders of magnitude in frequency (100,000–0.1 Hz) with a 10 millivolt alternating current excitation. A climate-controlled test chamber maintained the measurement environment at 25 °C (±1 °C tolerance), with all data acquired using an Admiral Squid Plot electrochemical workstation equipped with advanced frequency response analysis modules.

2.4. Material Characterization

The synthesized $LiMn_2O_4$ was examined using XRD (Rigaku SmartLab, Cu Kα radiation, λ = 1.5406 Å) operated at 40 kV and 40 mA. Diffraction patterns were recorded from 10°–80° (2θ) with a step size of 0.02° and a scan rate of 1 °/min. Rietveld refinement was applied for phase quantification. Morphological analysis was conducted via FE-SEM (Hitachi SU-8010) at 5–15 kV accelerating voltage to study particle size and surface morphology.

3. Results and Disscussion

The XRD pattern (Figure 5) exhibits characteristic diffraction peaks at 2θ positions corresponding to (010), (110), (011), (120), (200), and (021) crystallographic planes, which show excellent agreement with the reference pattern for spinel $LiMn_2O_4$ (JCPDS 35-0782). The peak positions and relative intensities confirm the successful formation of a phase-pure cubic spinel structure (space group Fd3m) without detectable secondary phases or impurities. The sharp and well-defined peaks indicate high crystallinity of the synthesized material, while the absence of peak broadening suggests minimal lattice strain [46]. This structural purity achieved through the sol-gel synthesis method is particularly noteworthy, as it demonstrates the method's effectiveness in controlling stoichiometry and preventing the formation of common impurity phases such as Mn_2O_3 or Li_2MnO_3 that often occur in high-temperature synthesis routes.

The SEM micrographs reveal a unique morphological characteristic where primary nanoparticles (~10 nm diameter) are interconnected through sintering necks, forming larger agglomerates (Figure 5). This nanostructured morphology results from the controlled thermal

decomposition of the gel precursor during calcination, where surface diffusion processes lead to particle fusion while preserving nanoscale features. The observed particle connectivity is advantageous for electrochemical applications as it provides: (1) short lithium-ion diffusion pathways due to the nanoscale primary particles [47], (2) enhanced electronic conductivity through the fused particle network [48], and (3) sufficient mechanical stability to withstand electrode fabrication processes [49]. The absence of distinct grain boundaries between primary particles suggests solid-state diffusion occurred during thermal treatment, which is consistent with the high crystallinity observed in XRD. The combination of XRD and SEM results demonstrates that the sol-gel synthesis produced phase-pure $LiMn_2O_4$ with optimal structural and morphological characteristics for energy storage applications. The nanoscale architecture with interconnected particles balances the often-competing requirements of high surface area (beneficial for charge transfer) and good structural integrity (necessary for cycling stability). These findings validate the sol-gel approach as an effective synthesis strategy for producing high-quality spinel cathode materials with controlled nanostructures.

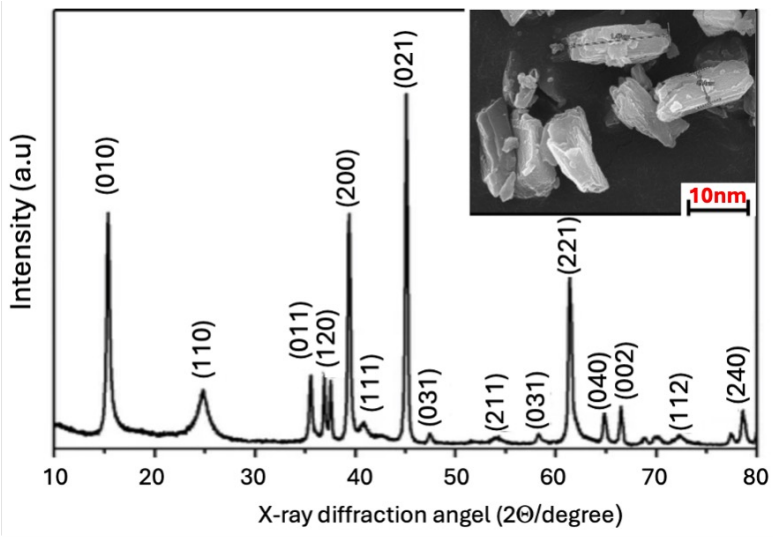

Figure 5. XRD pattern and SEM micrographs of sol-gel synthesized $LiMn_2O_4$.

The cyclic voltammetry results demonstrate the dual-ion electrochemical activity of $LiMn_2O_4$ in ammonium-containing electrolyte, where the first anodic scan (0.4-1.2 V vs Ag/AgCl) shows lithium extraction via $LiMn_2O_4 \rightarrow xLi^+ + Li_{1-x}Mn_2O_4 + xe^-$, evidenced by the stable ~0.004 mA peak current that persists through cycles, confirming the spinel framework's structural integrity during deintercalation (Figure 6). The subsequent cathodic scan (0.6-0.2 V) reveals NH_4^+ intercalation through $yNH_4^+ + Li_{1-x}Mn_2O_4 + ye^- \rightarrow (NH_4)_yLi_{1-x}Mn_2O_4$, characterized by a broad reduction peak suggesting a complex insertion mechanism involving Mn^{3+}/Mn^{4+} redox and possible hydrogen bonding with the spinel oxygen lattice. The quasi-reversible behavior (~100 mV peak separation) indicates kinetic limitations likely from NH_4^+ desolvation, while the gradually decreasing current implies progressive electrode activation. The overlapping redox signatures and sustained background current between 0.6-1.0 V reveal competing Li^+/NH_4^+ exchange processes and continuous surface reactions, yet the minimal (<30 mV) inter-cycle peak shifting confirms remarkable structural stability of the host framework during these dual-

ion storage operations. These findings collectively highlight $LiMn_2O_4$'s unique capability to accommodate both Li^+ extraction and NH_4^+ insertion while maintaining crystallographic integrity, making it promising for novel energy storage systems utilizing mixed-ion charge compensation mechanisms.

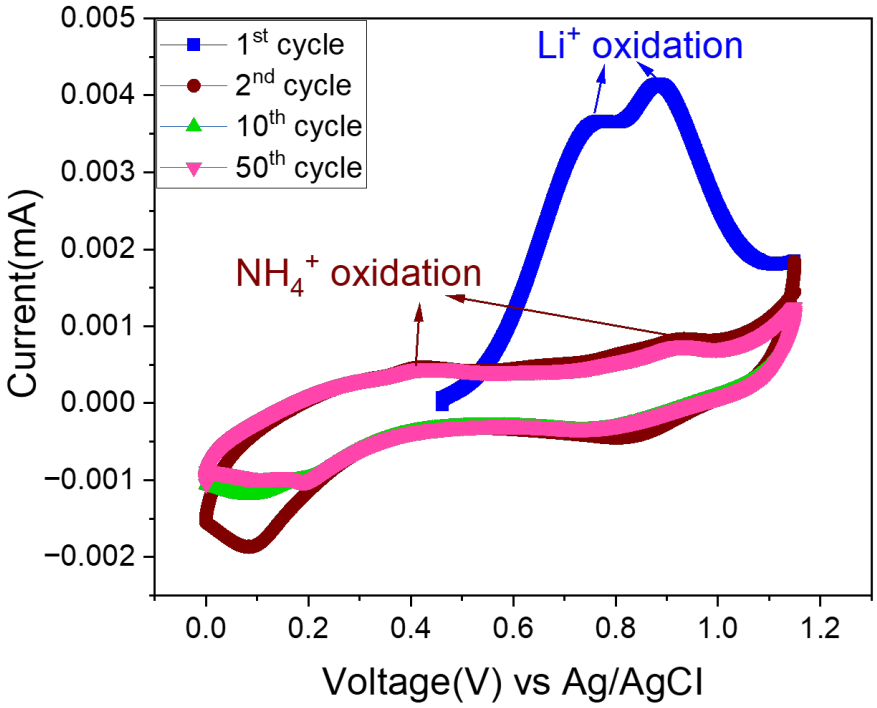

Figure 6. 1st and 2nd , 10th and 50th CV curves of $LiMn_2O_4$ in 1M $(NH_4)_2SO_4$ electrolyte at 1mV/s.

The galvanostatic charge/discharge results demonstrate a significant influence of electrolyte concentration on the electrochemical performance of the cathode material (Figure 7). The tests were conducted at different electrolyte concentrations ranging from 0.5 M to 4.0 M, revealing a clear correlation between electrolyte concentration and electrochemical performance. At the lowest concentration of 0.5 M, the battery delivers a discharge capacity of approximately 10 $mAhg^{-1}$, indicating insufficient lithium-ion transport and poor electrochemical utilization of the active material (Figure 7a). As the electrolyte concentration increases to 1.0 M, the discharge capacity improves slightly to around 15 $mAhg^{-1}$, suggesting an enhancement in ionic conductivity but still limited electrochemical activity (Figure 7b). A more significant improvement is observed at 2.0 M, where the discharge capacity reaches approximately 35 $mAhg^{-1}$, demonstrating the positive impact of increased ion availability and reduced charge-transfer resistance (Figure 7c). The best performance is achieved at 4.0 M, where the battery delivers a discharge capacity of nearly 60 $mAhg^{-1}$, indicating optimal lithium-ion transport and improved electrode kinetics (Figure 7d). Coulombic efficiency also shows a strong dependence on electrolyte concentration. At 0.5 M, the coulombic efficiency is relatively low, exhibiting fluctuations in the initial cycles before stabilizing at suboptimal levels. As the electrolyte concentration increases, coulombic efficiency improves, reaching near 100% at 2.0 M and 4.0 M, highlighting reduced side reactions and enhanced charge storage efficiency. The charge-

discharge capacity difference also decreases with increasing electrolyte concentration, suggesting improved electrochemical reversibility and reduced polarization effects.

From a mechanistic perspective, the improved performance at higher electrolyte concentrations is attributed to enhanced ion transport and reduced charge-transfer resistance at the cathode-electrolyte interface [49]. At lower concentrations (0.5 M and 1.0 M), the limited availability of charge carriers results in poor capacity retention and increased side reactions, leading to irreversible capacity loss. The significant improvement at 2.0 M and 4.0 M suggests that higher ionic conductivity facilitates better lithium-ion mobility, ensuring efficient charge transfer and minimizing losses due to internal resistance [51]. Furthermore, the structural integrity of the cathode material appears to be well-maintained at higher concentrations, preventing severe degradation and prolonging cycle life. However, while 4.0 M delivers the highest discharge capacity, excessively high electrolyte concentrations may lead to increased viscosity, which could introduce limitations in practical applications. Overall, the results confirm that electrolyte concentration is a critical parameter influencing battery performance. The increase from 0.5 M to 4.0 M leads to a substantial enhancement in discharge capacity, coulombic efficiency, and long-term stability, with an optimal balance observed at higher concentrations. Fine-tuning electrolyte concentration is essential for optimizing energy storage performance, particularly for applications requiring high capacity, stable cycling, and minimal degradation [52].

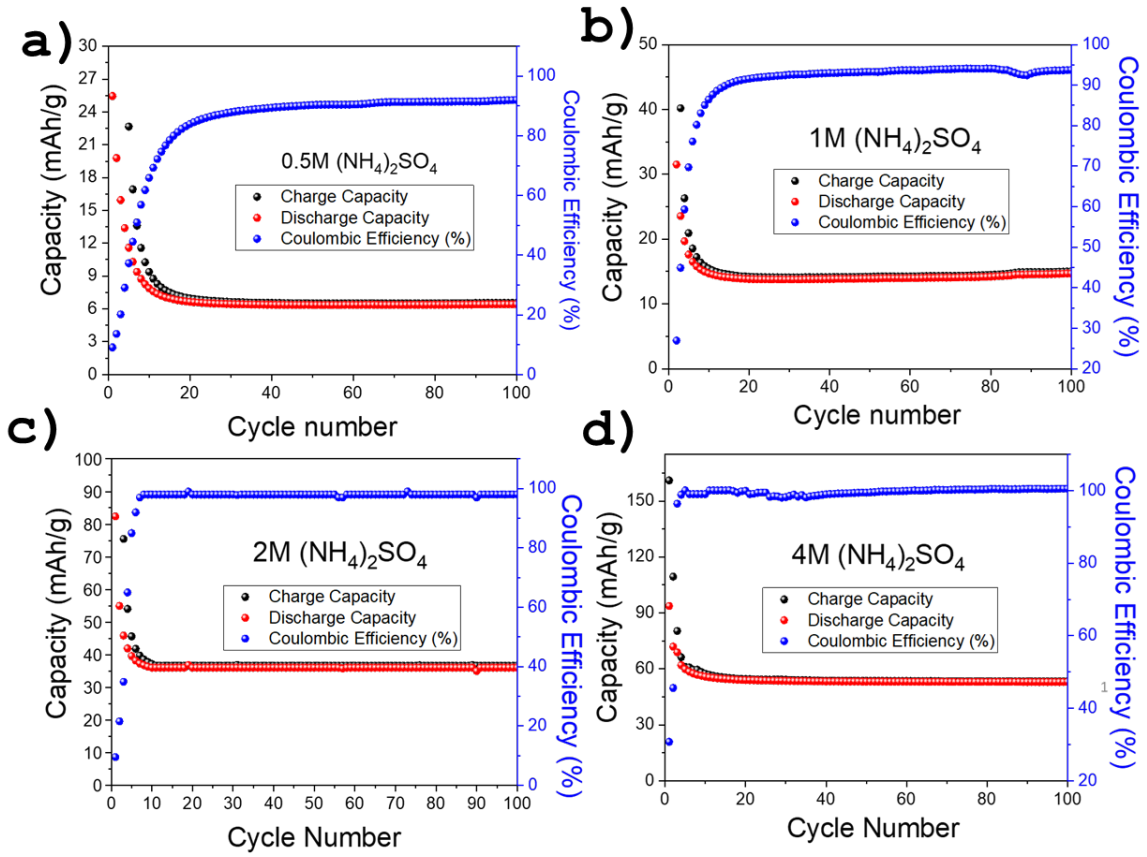

Figure 7. Galvanostatic charge-discharge performance of the cathode material ($LiMn_2O_4$) at different electrolyte concentrations : a) 0.5M $(NH_4)_2SO_4$, b) 1M $(NH_4)_2SO_4$, c) 2M $(NH_4)_2SO_4$, and d) 4M $(NH_4)_2SO_4$.

The theoretical ionic conductivity (κ) of $(NH_4)_2SO_4$ electrolyte was calculated at different concentrations (0.5M, 1.0M, 1.5M, and 2.0M) using the molar ionic conductivities at infinite dilution (Equation 1). The values for ammonium (NH_4^+) and sulfate (SO_4^{2-}) ions are 73.6 $S \cdot cm^2 \cdot mol^{-1}$ and 160.0 $S \cdot cm^2 \cdot mol^{-1}$, respectively. Upon dissolution in aqueous solution, $(NH_4)_2SO_4$ completely dissociates into two NH_4^+ cations and one SO_4^{2-} anion per formula unit. The ionic conductivity of the solution is then determined using the equation [53]:

$$\kappa = (2C \cdot \lambda^0 NH_4^+) + (C \cdot \lambda^0 SO_4^{2-}) \quad (1)$$

where C represents the bulk electrolyte concentration. Substituting the values into this equation, the calculated ionic conductivities for different molar concentrations are as follows: 153.6 $S \cdot cm^2 mol^{-1}$ for 0.5M, 307.2 $S \cdot cm^2 \cdot mol^{-1}$ for 1.0M, 460.8 $S \cdot cm^2 mol^{-1}$ for 1.5M, and 614.4 $S \cdot cm^2 mol^{-1}$ for 2.0M (Table 1). These theoretical values assume ideal conditions, where ions are fully dissociated and independent in solution, as described by Kohlrausch's Law of Independent Migration of Ions [54]. However, in real electrochemical systems, deviations from ideal behavior occur at higher concentrations due to ion pairing, electrostatic interactions, and reduced ion mobility. At increased ionic strength, conductivity typically reaches a maximum and then decreases due to the formation of ion clusters, which reduces the number of free charge carriers available for conduction. This phenomenon is particularly relevant for high-concentration electrolyte applications such as batteries, supercapacitors, and electrochemical capacitors. Understanding the ionic conductivity of $(NH_4)_2SO_4$ is essential for evaluating its suitability as an electrolyte in energy storage devices [54]. Higher ionic conductivity generally improves charge transport, enhancing electrode kinetics and overall device performance. These results indicate that $(NH_4)_2SO_4$ exhibits high ionic conductivity, making it a promising candidate for electrochemical applications.

Table 1. Theoretical Ionic Conductivity of $(NH_4)_2SO_4$ Electrolyte at Different Concentrations

Concentration (M)	Theoretical Ionic Conductivity ($S \cdot cm^2 \cdot mol^{-1}$)
0.5	153.6
1.0	307.2
2	614.4
4	1228.8

The cyclic voltammetry (CV) curves recorded at different scan rates (10, 20, 40, and 60 mV/s) show a clear increase in peak current as the scan rate increases (Figure 8a). This behavior indicates a diffusion-controlled charge transfer process, which aligns with the Randles-Sevcik equation (Equation 2) [55]:

$$i_p = (2.69 * 10^5) * n^{3/2} A * C * D^{1/2} * v^{1/2} \quad (2)$$

In this equation, i_p denotes the peak current, C refers to the molar concentration of electroactive species, n indicates the electron transfer count per redox reaction, A corresponds to the geometric surface area of the electrode, D signifies the mass transport diffusion coefficient, and v defines the applied potential sweep rate. The linear relationship observed between the peak current and the square root of the scan rate confirms that the NH_4^+ ion diffusion governs the charge storage process. According to this equation, the peak current (i_p) is proportional to the square root of the scan rate ($v^{1/2}$), confirming that the movement of NH_4^+ ions within the $LiMn_2O_4$ electrode is primarily governed by diffusion (Figure 8b). The observed trend suggests that ion transport efficiency is directly influenced by the applied scan rate, affecting the overall electrochemical response of the electrode. The calculated diffusion coefficients for NH_4^+ ions during oxidation and reduction exhibit some variations. The values obtained—$D_1 = 1.23 \times 10^{-5}$ $cm^2\ s^{-1}$, $D_2 = 2.214 \times 10^{-5}$ $cm^2 s^{-1}$, $D_3 = 1.59 \times 10^{-5}$ $cm^2\ s^{-1}$, and $D_4 = 2.76 \times 10^{-5}$ $cm^2\ s^{-1}$—indicate that ion mobility is not uniform across different potential regions. Higher diffusion coefficients (D_2 and D_4) suggest that NH_4^+ ions move more efficiently in specific electrochemical conditions, possibly due to structural changes in the $LiMn_2O_4$ lattice or alterations in interfacial charge transfer kinetics. The variations in diffusion coefficients highlight the complex nature of NH_4^+ ion transport and suggest that external factors such as electrode porosity and electrolyte interactions may play a role. A noticeable asymmetry exists between the diffusion coefficients obtained during the anodic and cathodic sweeps, implying that NH_4^+ insertion and extraction processes are not entirely reversible. This difference may arise from structural modifications occurring in $LiMn_2O_4$ as the electrode undergoes charge-discharge cycling. Additionally, changes in solvation and desolvation rates of NH_4^+ ions could influence the charge transfer kinetics, leading to variations in diffusion behavior. Higher diffusion coefficient of D2 and D4 redox couple suggests that higher diffusion coefficients (D_2 and D_4) suggest that NH_4^+ ions move more efficiently in specific electrochemical conditions, possibly due to structural changes in the $LiMn_2O_4$ lattice or alterations in interfacial charge transfer kinetics. The observed diffusion coefficients provide valuable insights into the electrochemical performance of $LiMn_2O_4$ in 4M $(NH_4)_2SO_4$ electrolyte. The relatively high ion mobility indicates that this system could be a promising candidate for ammonium-ion-based energy storage applications. However, the variations in diffusion coefficients suggest that further optimization of the electrode structure and composition could enhance the uniformity of ion transport and improve overall performance. Addressing these inconsistencies through material modifications or electrolyte engineering could lead to more efficient and stable charge storage systems. In conclusion, the diffusion of NH_4^+ ions within the $LiMn_2O_4$ electrode follows a diffusion-controlled mechanism, as confirmed by the Randles-Sevcik equation. The differences in diffusion coefficients suggest that NH_4^+ ion transport is influenced by potential-dependent structural changes and interfacial interactions [56]. Higher diffusion coefficients in certain regions indicate favorable ion movement, which could be leveraged for fast charge-discharge applications. Further research into electrode stability and electrolyte optimization may help enhance the performance of $LiMn_2O_4$ for ammonium-ion battery technologies.

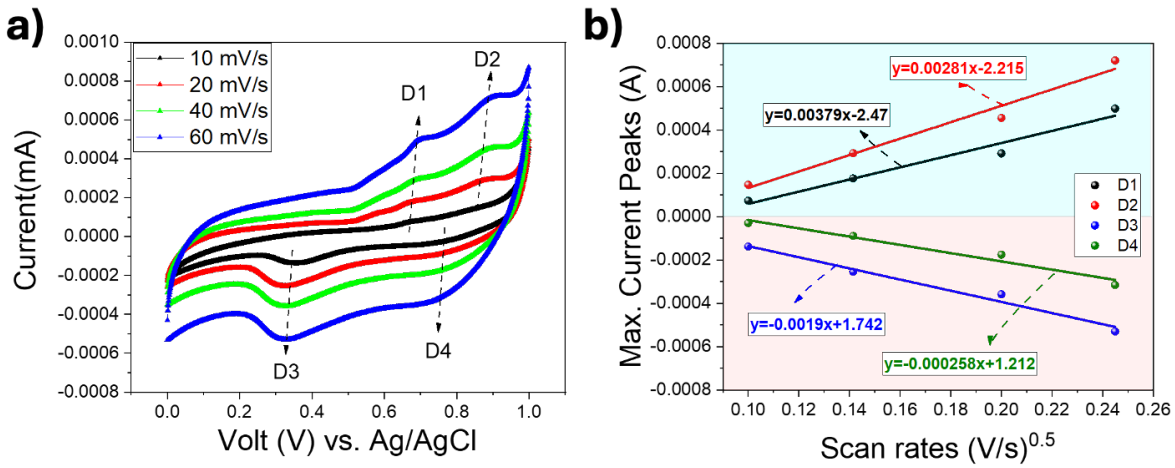

Figure 8. Electrochemical characterization of charge storage behavior: a) Potential-dependent current response measured at varying potential sweep rates (10–60 mV/s), demonstrating redox activity under dynamic conditions. b) Quantitative diffusion analysis showing the linear relationship between peak current densities (I_p) and the square root of scan rate ($v^{1/2}$) for four distinct redox processes (designated D1–D4).

The charge-discharge profiles of the $LiMn_2O_4$ electrode in 4M $(NH_4)_2SO_4$ electrolyte, as shown in Figure 9a, demonstrate superior electrochemical performance across different current densities. At 1C, the electrode delivers a high cumulative capacity of approximately 55 mAh/g, which remains relatively stable even at higher rates. At 2C, 4C, and 8C, the capacity retention is still significant, maintaining values around 45 $mAhg^{-1}$, 38 $mAhg^{-1}$, and 30 $mAhg^{-1}$, respectively. Even at the extreme rate of 10C, the electrode retains approximately 25 $mAhg^{-1}$, indicating excellent rate capability. The well-defined voltage plateaus observed in the charge-discharge curves suggest stable redox reactions and efficient NH_4^+ ion insertion/extraction within the electrode structure. The ability to sustain a high capacity at fast charge/discharge rates implies that the 4M $(NH_4)_2SO_4$ electrolyte provides enhanced ionic transport, facilitating rapid electrochemical kinetics.

The electrochemical impedance spectroscopy (EIS) results in Figure 9b further confirm this conclusion. The Nyquist plots show that the charge transfer resistance (R_{ct}) is significantly reduced in 4M $(NH_4)_2SO_4$ compared to lower concentrations. The fitted R_{ct} values for 0.5M, 1M, 2M, and 4M electrolytes are approximately 200 Ω, 120 Ω, 50 Ω, and 20 Ω, respectively. This drastic decrease in charge transfer resistance at 4M indicates improved ion conductivity and faster charge transfer at the electrode-electrolyte interface. Additionally, the high-frequency semicircle, representing charge transfer resistance, is smallest for the 4M electrolyte, suggesting minimal polarization effects.

The previously calculated theoretical ionic conductivity values for 0.5M, 1.0M, 2.0M, and 4.0M are 153.6 $S{\cdot}cm^2mol^{-1}$, 307.2 $S{\cdot}cm^2mol^{-1}$, 614.4 $S{\cdot}cm^2mol^{-1}$, and 1228.8 $S{\cdot}cm^2mol^{-1}$, respectively. The high ionic conductivity of the 4M electrolyte ensures sufficient NH_4^+ ion availability for charge transport, reducing ohmic losses and enhancing reaction kinetics. This improvement directly contributes to the enhanced electrochemical performance observed in the

charge-discharge tests (Figure 9a) and EIS results (Figure 9b). These findings emphasize the critical role of electrolyte concentration in optimizing the electrochemical behavior of $LiMn_2O_4$ electrodes. The high ionic strength of the 4M electrolyte minimizes diffusion limitations, reduces polarization, and supports high-rate performance. However, further studies on long-term cycling stability and potential electrode degradation at high electrolyte concentrations are necessary to confirm its suitability for practical applications. The observed electrochemical improvements suggest that concentrated $(NH_4)_2SO_4$ electrolytes hold great promise for high-power ammonium-ion-based energy storage devices.

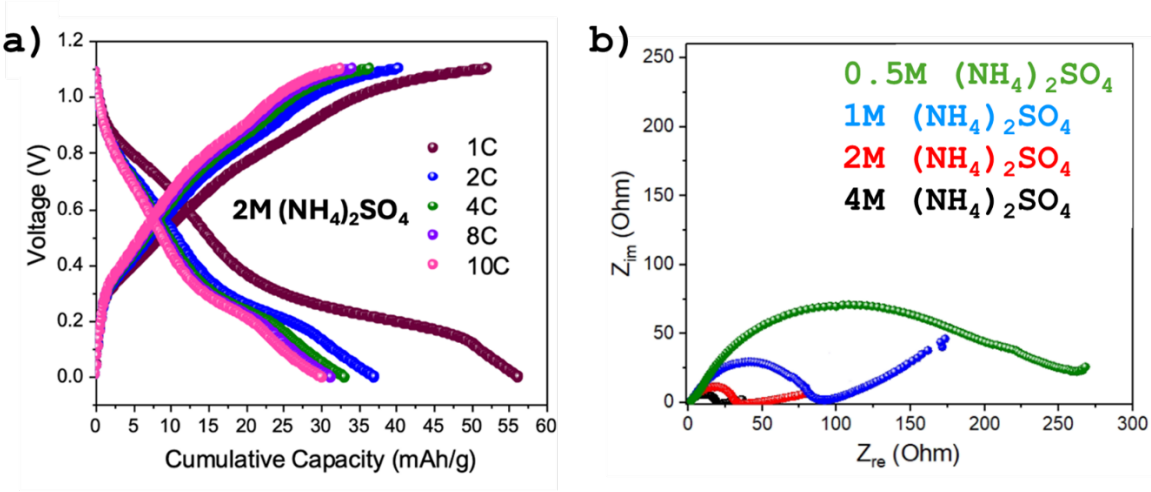

Figure 9. a) The first discharge performances of $LiMn_2O_4$ in 4M $(NH_4)_2SO_4$ at different C-rates, b) Nyquist-plot curves of $LiMn_2O_4$ in different concentrations of aqueous $(NH_4)_2SO_4$ electrolyte.

4. Conclusion

This study demonstrates the exceptional electrochemical performance of $LiMn_2O_4$ as a cathode material in ammonium-ion-based energy storage systems using $(NH_4)_2SO_4$ electrolyte. The XRD results confirm the successful synthesis of a highly crystalline, phase-pure spinel $LiMn_2O_4$ structure (JCPDS 35-0782), while SEM analysis reveals a nanostructured morphology with interconnected primary nanoparticles (~10 nm), enhancing lithium-ion transport and electronic conductivity. The dual-ion electrochemical activity observed in cyclic voltammetry (CV) confirms the capability of $LiMn_2O_4$ to undergo reversible Li^+ extraction and NH_4^+ insertion, maintaining structural integrity with minimal peak shifts (<30 mV) over multiple cycles. The electrochemical performance exhibits a strong dependence on electrolyte concentration. Charge-discharge analysis reveals that increasing the electrolyte concentration from 0.5 M to 4.0 M significantly enhances the discharge capacity from ~10 $mAhg^{-1}$ to ~60 $mAhg^{-1}$, demonstrating improved ion transport, reduced polarization, and higher coulombic efficiency (~100% at 2.0 M and 4.0 M). Electrochemical impedance spectroscopy (EIS) further corroborates these findings, showing a drastic reduction in charge transfer resistance (R_{ct}) from ~200 Ω (0.5 M) to ~20 Ω (4.0 M), indicative of enhanced interfacial charge transport. The theoretical ionic conductivity calculations align well with experimental trends, highlighting the importance of electrolyte concentration in optimizing ionic mobility and minimizing resistance

losses. Scan rate-dependent CV studies confirm that the NH_4^+ ion transport follows a diffusion-controlled process, with diffusion coefficients ranging from 1.23×10^{-5} cm^2s^{-1} to 2.76×10^{-5} cm^2s^{-1}, depending on the electrochemical conditions. The variations in diffusion coefficients suggest potential electrode-electrolyte interactions and structural modifications that influence NH_4^+ transport kinetics. Despite minor kinetic limitations associated with NH_4^+ desolvation, the $LiMn_2O_4$ electrode demonstrates excellent rate capability, retaining a substantial capacity (~25 $mAhg^{-1}$) even at high charge/discharge rates (10C), underscoring its suitability for fast-charging applications.

Collectively, these results demonstrate $LiMn_2O_4$'s strong potential as an advanced cathode material for NH_4^+-based energy storage systems, owing to its robust crystalline framework, engineered nanoscale architecture, and synergistic cation storage behavior. The 4M ammonium sulfate electrolyte formulation achieves an optimal compromise between ionic mobility, interfacial charge transfer efficiency, and electrode integrity, positioning it as a leading candidate for high-rate energy storage devices. Subsequent research efforts should prioritize: (i) extended operational durability assessment, (ii) fundamental understanding of capacity fade mechanisms, and (iii) advanced electrolyte engineering to maximize both performance metrics and commercial feasibility. These advances provide a foundation for designing innovative electrochemical storage technologies based on ammonium-ion chemistry that combine high energy density, superior power characteristics, and exceptional longevity.

Ethics in Publishing

There are no ethical issues regarding the publication of this study.

Author Contributions

Melisa Uçan and Dilara Özgenc performed the experimental studies, including material synthesis and electrochemical measurements. Yıldıray Topçu contributed to the writing and critical revision of the manuscript. Burak Tekin designed the study, conducted material characterization and electrochemical analyses, wrote the manuscript, and interpreted the results. All authors reviewed and approved the final version of the paper.

Acknowledgements

We would like to thank the Electrochemical Conversion and Storage Laboratory for their support with the electrochemical measurements and the Black sea Advanced Research Center for conducting the XRD and SEM analyses.

References

[1] Abas, N., Kalair, A., & Khan, N. (2015). Review of fossil fuels and future energy technologies. *Futures, 69*, 31-49.

[2] Zou, C., Zhao, Q., Zhang, G., & Xiong, B. (2016). Energy revolution: From a fossil energy era to a new energy era. *Natural Gas Industry B, 3*(1), 1-11.

[3] Notton, G., Nivet, M.-L., Voyant, C., Paoli, C., Darras, C., Motte, F., & Fouilloy, A. (2018). Intermittent and stochastic character of renewable energy sources: Consequences, cost of intermittence and benefit of forecasting. *Renewable and Sustainable Energy Reviews, 87*, 96-105.

[4] Wu, Y., Wang, W., Ming, J., Li, M., Xie, L., He, X., ... & Wu, Y. (2019). An exploration of new energy storage system: High energy density, high safety, and fast charging lithium ion battery. *Advanced Functional Materials, 29*(1), 1805978.

[5] Sayed, E. T., Olabi, A. G., Alami, A. H., Radwan, A., Mdallal, A., Rezk, A., & Abdelkareem, M. A. (2023). Renewable energy and energy storage systems. *Energies, 16*(3), 1415.

[6] Mitali, J., Dhinakaran, S., & Mohamad, A. (2022). Energy storage systems: A review. *Energy Storage and Saving, 1*(3), 166-216.

[7] Christen, T., & Carlen, M. W. (2000). Theory of Ragone plots. *Journal of Power Sources, 91*(2), 210-216.

[8] Christen, T., & Ohler, C. (2002). Optimizing energy storage devices using Ragone plots. *Journal of Power Sources, 110*(1), 107-116.

[9] Pell, W., & Conway, B. (1996). Quantitative modeling of factors determining Ragone plots for batteries and electrochemical capacitors. *Journal of Power Sources, 63*(2), 255-266.

[10] Larcher, D., & Tarascon, J.-M. (2015). Towards greener and more sustainable batteries for electrical energy storage. *Nature Chemistry, 7*(1), 19-29.

[11] Goodenough, J. B. (2013). Evolution of strategies for modern rechargeable batteries. *Accounts of Chemical Research, 46*(5), 1053-1061.

[12] Olabi, A. G., Abbas, Q., Shinde, P. A., & Abdelkareem, M. A. (2023). Rechargeable batteries: Technological advancement, challenges, current and emerging applications. *Energy, 266*, 126408.

[13] Boddula, R., Pothu, R., & Asiri, A. M. (2020). *Rechargeable Batteries: History, Progress, and Applications*. John Wiley & Sons.

[14] Nekahi, A., Madikere Raghunatha Reddy, A. K., Li, X., Deng, S., & Zaghib, K. (2025). Rechargeable Batteries for the Electrification of Society: Past, Present, and Future. *Electrochemical Energy Reviews, 8*(1), 1-30.

[15] Liang, Y., Zhao, C.-Z., Yuan, H., Chen, Y., Zhang, W., Huang, J.-Q., ... & Chueh, Y.-L. (2019). A review of rechargeable batteries for portable electronic devices. *InfoMat, 1*(1), 6-32.

[16] Mauger, A., & Julien, C. (2017). Critical review on lithium-ion batteries: Are they safe? Sustainable? *Ionics, 23*, 1933-1947.

[17] Wu, X., Song, K., Zhang, X., Hu, N., Li, L., Li, W., ... & Zhang, H. (2019). Safety issues in lithium ion batteries: Materials and cell design. *Frontiers in Energy Research, 7*, 65.

[18] Han, J., Varzi, A., & Passerini, S. (2022). The emergence of aqueous ammonium-ion batteries. *Angewandte Chemie, 134*(14), e202115046.

[19] Wang, Y., & Kuchena, S. F. (2022). Recent progress in aqueous ammonium-ion batteries. *ACS Omega, 7*(38), 33732-33748.

[20] Zhang, R., Wang, S., Chou, S., & Jin, H. (2022). Research development on aqueous ammonium-ion batteries. *Advanced Functional Materials, 32*(25), 2112179.

[21] Tekin, B., Sevinc, S., Morcrette, M., & Demir-Cakan, R. (2017). A new sodium-based aqueous rechargeable battery system: The special case of $Na_{0.44}MnO_2$/dissolved sodium polysulfide. *Energy Technology, 5*(12), 2182-2188.

[22] Sevinc, S., Tekin, B., Ata, A., Morcrette, M., Perrot, H., Sel, O., & Demir-Cakan, R. (2019). In-situ tracking of NaFePO4 formation in aqueous electrolytes and its electrochemical performances in Na-ion/polysulfide batteries. *Journal of Power Sources, 412*, 55-62.

[23] Pahari, D., & Puravankara, S. (2020). Greener, safer, and sustainable batteries: An insight into aqueous electrolytes for sodium-ion batteries. *ACS Sustainable Chemistry & Engineering, 8*(29), 10613-10625.

[24] Chen, S., Zhang, M., Zou, P., Sun, B., & Tao, S. (2022). Historical development and novel concepts on electrolytes for aqueous rechargeable batteries. *Energy & Environmental Science, 15*(5), 1805-1839.

[25] Zhang, H., Liu, X., Li, H., Hasa, I., & Passerini, S. (2021). Challenges and strategies for high-energy aqueous electrolyte rechargeable batteries. *Angewandte Chemie International Edition, 60*(2), 598-616.

[26] Dell, R. (1996). Aqueous electrolyte batteries. *Philosophical Transactions of the Royal Society of London. Series A: Mathematical, Physical and Engineering Sciences, 354*(1712), 1515-1527.

[27] Zhang, Q., Yang, Z., Ji, H., Zeng, X., Tang, Y., Sun, D., & Wang, H. (2021). Issues and rational design of aqueous electrolyte for Zn-ion batteries. *SusMat, 1*(3), 432-447.

[28] Li, X., Liu, P., Han, C., Cai, T., Cui, Y., Xing, W., & Zhi, C. (2025). Corrosion of metallic anodes in aqueous batteries. *Energy & Environmental Science*.

[29] Sun, Y., Yin, B., Yang, J., Ding, Y., Li, M., Li, H., ... & Ma, T. (2023). Ammonium-ion energy storage devices for real-life deployment: Storage mechanism, electrode design and system integration. *Energy & Environmental Science, 16*(12), 5568-5604.

[30] Zheng, R., Li, Y., Yu, H., Zhang, X., Yang, D., Yan, L., ... & Su, B. L. (2023). Ammonium ion batteries: Material, electrochemistry and strategy. *Angewandte Chemie, 135*(23), e202301629.

[31] Tawalbeh, M., Murtaza, S. Z., Al-Othman, A., Alami, A. H., Singh, K., & Olabi, A. G. (2022). Ammonia: A versatile candidate for the use in energy storage systems. *Renewable Energy, 194*, 955-977.

[32] Tian, Z. (2024). *Designing Advanced Aqueous Ammonium-Ion Batteries by Hydrogen-Bond Chemistry*.

[33] Li, C., Yan, W., Liang, S., Wang, P., Wang, J., Fu, L., ... & Huang, W. (2019). Achieving a high-performance Prussian blue analogue cathode with an ultra-stable redox reaction for ammonium ion storage. *Nanoscale Horizons, 4*(4), 991-998.

[34] Xing, J., Fu, X., Guan, S., Zhang, Y., Lei, M., & Peng, Z. (2021). Novel KV-Fe Prussian blue analogues nanocubes for high-performance aqueous ammonium ion batteries. *Applied Surface Science, 543*, 148843.

[35] Li, S., Xia, M., Xiao, C., Zhang, X., Yu, H., Zhang, L., & Shu, J. (2021). Common ion effect enhanced Prussian blue analogues for aqueous ammonium ion storage. *Dalton Transactions, 50*(19), 6520-6527.

[36] Zhang, Y., An, Y., Yin, B., Jiang, J., Dong, S., Dou, H., & Zhang, X. (2019). A novel aqueous ammonium dual-ion battery based on organic polymers. *Journal of Materials Chemistry A, 7*(18), 11314-11320.

[37] Zhang, Y., Yao, Q., Sun, Y., Zhao, Y., & Niu, Y. (2024). Multifunctional Porous Organic Polymer Anode with Desired Redox Potential and Capacity for High-Performance Aqueous Sodium-Ion and Ammonium-Ion Batteries. *ACS Applied Materials & Interfaces, 16*(40), 53688-53696.

[38] Shi, M., Zhang, Y., Zhou, X., Li, Y., Xiao, S., Liu, S., ... & Li, Y. (2023). A high-energy/power and ultra-stable aqueous ammonium ion microbattery based on amorphous/crystalline dual-phase layered metal oxides. *Chemical Engineering Journal, 464*, 142600.

[39] Song, Y., Pan, Q., Lv, H., Yang, D., Qin, Z., Zhang, M. Y., ... & Liu, X. X. (2021). Ammonium-ion storage using electrodeposited manganese oxides. *Angewandte Chemie, 133*(11), 5782-5786.

[40] Erraji, A., Masrour, R., & Xu, L. (2024). Ab initio study of $LiMn_2O_4$ cathode: Electrochemical and optical properties for Li-ion batteries and optoelectronic devices. *Ionics, 30*(12), 7917-7928.

[41] Ghosh, S., Bhattacharjee, U., Bhowmik, S., and Martha, S.K. (2022). A Review on High-Capacity and High-Voltage Cathodes for Next-Generation Lithium-ion Batteries. Journal of Energy and Power Technology, 4(1), 2-59.

[42] Tiruvannamalai Annamalai, A. K. (2007). *Chemical, structural, and electrochemical characterization of 5 V spinel and complex layered oxide cathodes of lithium ion batteries*.

[43] Jia, L. (2016). *Spinel-based cathode materials for high energy/power lithium ion batteries*. National University of Singapore (Singapore).

[44] Stoyanova, R., Koleva, V., & Stoyanova, A. (2019). Lithium versus Mono/Polyvalent ion intercalation: Hybrid metal ion systems for energy storage. *The Chemical Record, 19*(2-3), 474-501.

[45] Wu, H., Luo, S., Wang, H., Li, L., Fang, Y., Zhang, F., ... & Yuan, W. (2024). A review of anode materials for dual-ion batteries. *Nano-Micro Letters, 16*(1), 252.

[46] Zhang, M., Sun, C., Li, J., Shi, C., Li, X., & Zhao, B. (2025). Suppressed Mn dissolution behavior to improve cycling performance of Cr-modified $Li_{1-x}Mn_2O_4$ electrodes. *Colloids and Surfaces A: Physicochemical and Engineering Aspects, 136283*.

[47] Wang, F., Yu, H.-C., Chen, M.-H., Wu, L., Pereira, N., Thornton, K., ... & Graetz, J. (2012). Tracking lithium transport and electrochemical reactions in nanoparticles. *Nature Communications, 3*(1), 1201.

[48] Aikiyo, H., Nakane, K., Ogata, N., & Ogihara, T. (2001). Effect of particle morphology on electrochemical property of $LiMn_2O_4$. *Journal of the Ceramic Society of Japan, 109*(1270), 506-510.

[49] Shin, S. Y. (2015). *Electrochemical and mechanical properties of $LiMn_2O_4$ according to particle morphology*. Seoul National University.

[50] Kondo, Y., Abe, T., & Yamada, Y. (2022). Kinetics of interfacial ion transfer in lithium-ion batteries: Mechanism understanding and improvement strategies. *ACS Applied Materials & Interfaces, 14*(20), 22706-22718.

[51] Chandra, A., & Bagchi, B. (2000). Frequency dependence of ionic conductivity of electrolyte solutions. *The Journal of Chemical Physics, 112*(4), 1876-1886.

[52] Liu, X., Fan, K., Huang, X., Ge, J., Liu, Y., & Kang, H. (2024). Recent advances in artificial intelligence boosting materials design for electrochemical energy storage. *Chemical Engineering Journal, 151625*.

[53] Wright, M. R. (2007). *An introduction to aqueous electrolyte solutions*. John Wiley & Sons.

[54] Picálek, J., & Kolafa, J. (2007). Molecular dynamics study of conductivity of ionic liquids: The Kohlrausch law. *Journal of Molecular Liquids, 134*(1-3), 29-33.

[55] El-Latif, E. I. A., Alahmadi, M., Kebede, M. A., Phasha, M., Hameed, T. A., Khairy, Y., ... & Sheha, E. (2024). *Modeling the Diffusion Coefficient of Charge Carriers in Batteries Using the Randles-Sevcik Equation*. Available at SSRN 4749003.

[56] Magnussen, O. M., & Groß, A. (2019). Toward an atomic-scale understanding of electrochemical interface structure and dynamics. *Journal of the American Chemical Society, 141*(12), 4777-4790.